Multi-Purpose Electronic Contactor Design with High-Side FET Driver, and Insulation Resistance Measurement

Emre Dincer[1-2], Tolga Baykal[2]

[1] *Institute of Defense Technologies, Gebze Technical University, Gebze-Kocaeli, 41400, Türkiye*
[2] *Togi Teknoloji San. ve Tic. Ltd. Şti. Bilişim Vadisi, Gebze-Kocaeli, 41400, Türkiye*

Abstract

This study presents an intelligent, compact electronic contactor system for electric vehicle (EV) batteries. It integrates high-side N-channel FET drivers for the charge, discharge, pre-charge, and pre-discharge paths. The pre-charge circuit is activated first when the battery is connected. It limits the inrush current through a high-resistance path to protect the power components. The pre-discharge circuit performs a similar role when the load is activated. Once stabilized, the system engages low-resistance charge and discharge paths to ensure efficient energy transfer. This process is monitored by a precision shunt resistor with a Kelvin connection (SRP/SRN), which enables accurate bilateral current sensing via the analog front end (AFE). Real-time insulation resistance monitoring, which complies with the 500 Ω/V safety threshold, is achieved through signal injection or bridge methods. This enables early fault detection under harsh conditions. To provide comprehensive system protection, programmable electronic fuses (eFuses) respond to overcurrent events in less than 100 µs using external current data from the AFE. These eFuses offer resettable, load-adaptive safety features that align with modern electrical/electronic (E/E) architectures. This integrated design enhances functional safety, measurement accuracy, and regulatory compliance while minimizing component size and system complexity.

Keywords: Charge; Discharge; Electronic Contactor; Pre-Charge; Pre-Discharge; Insulation Resistor Monitoring; Electronic Fuses

1. Introduction

In today's world, lithium batteries, which can reach high power and energy capacity, have brought with them the need for precise and continuous monitoring and the need to take trustworthy measures. These electrochemical energy sources, which must operate within a safe range of voltage, current and temperature levels, have also been standardized with a series of regulations to protect property and public safety [1-2]. In this study, an electronic contactor system capable of measuring insulation resistance has been developed to meet this safety requirement and facilitate compliance with the required standards. Insulation resistance measurement is a critical test for the safety, performance and longevity of lithium battery systems [3-8].

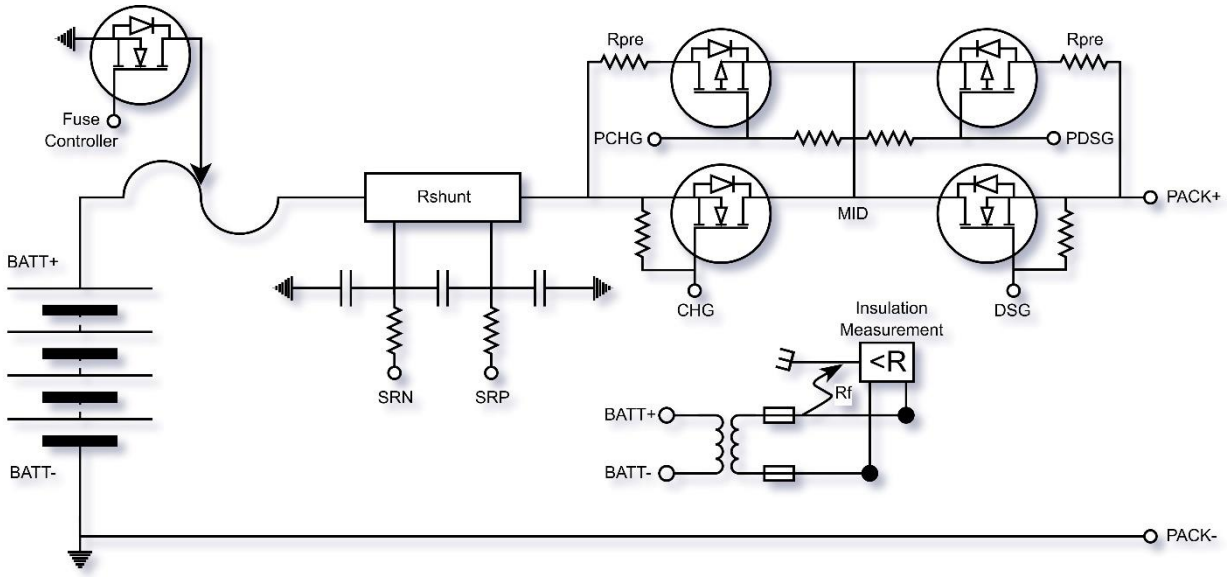

Figure 1. Schematic Design of Electronic Contactor

* *Corresponding author e-mail:ee.dinceremre@gmail.com*

The study begins with the control of current flow, one of the three fundamental quantities when it comes to lithium batteries, and the measurement of the magnitude that allows us to decide when and how to control this current. Traditionally, the current flowing through the main current paths is controlled by electromechanical elements that connect or disconnect the power path when necessary, stopping the flow of current [9-10]. However, this method has a number of drawbacks and in order to take a more innovative approach in this work, a FET based control circuit is designed using highside gate drivers for both charge and discharge directions and also for both pre-charge and pre-discharge paths [11-16].

One of the better ways of current measurement is to use Hall effect sensors, but although this method provides isolation and high current measurement capability, the measurement accuracy may be degraded due to magnetic losses, air gaps and external interferences. In this study, a compact, low-cost, and integrated method is used to measure current using a highpower shunt resistor with differentially matched Kelvin connections and digital filters. This method uses highresolution analog-to-digital converters (ADCs) to measure the current with high accuracy and can be used in SoX calculations to provide more accurate results [17].

In case of worst scenario such as crash, fire, external accident, the system may consist of fuse solutions such as eFuse, pyroFuse or DC fuse to ensure the power flow [18]. Fast-acting power elements increase the functional safety level of the system and the compactness of the power path controllers [19].

Table 1. Gate Algorithm (0: OFF, 1: ON)

Gate / Mode	PDSG (Pre-Discharge FET)	DSG (Discharge FET)	PCHG (Pre-Charge FET)	CHG (Charge FET)	e-Fuse Controller
Shutdown	0	0	0	0	0
Pre-Discharge	1	0	0	1	0
Discharge	0	1	0	1	0
Pre-Charge	0	1	1	0	0
Charge	0	1	0	1	0
Damage	0	0	0	0	1

2. Electronic Contactor Design

2.1. Transient Power Paths

Transient power paths carry the main current immediately after the system starts up. This current is requested from the battery. Depending on the characteristics of the load (ohmic, capacitive, or inductive), the current may exceed its nominal value before settling at a stable level. These paths are positioned with a series limiting resistor to avoid high-current damage to the battery and load. The same applies to the charging current supplied by the charging device to the battery as opposed to the current required by the load. Pre-discharge and pre-charge operations are critical for maintaining the health of the battery and load. These operations must be used in high-power battery systems to minimize loss of life and property.

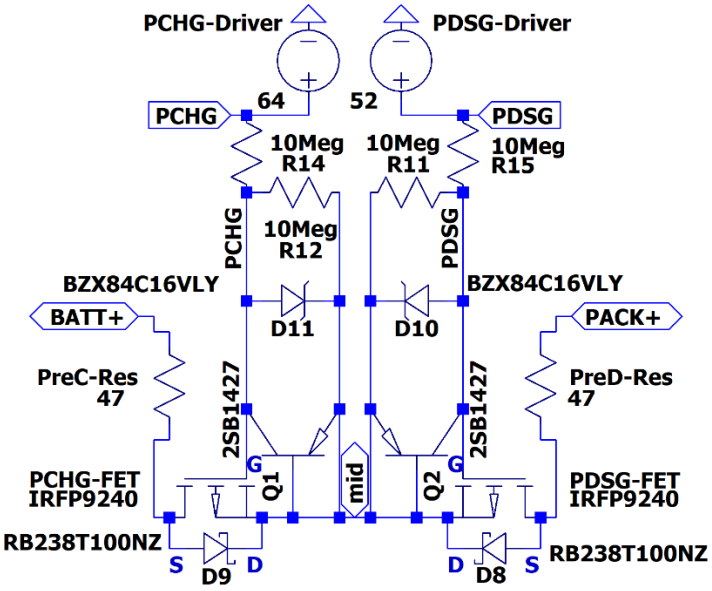

Figure 2. Schematic Design of Transient Power Paths

The corresponding gates (PDSG, DSG, PCHG and CHG), which align with the gate algorithms referenced in Table 1, are illustrated in Figure 1. FETs, where the current must pass through body diodes in both directions, are driven at 10V, as indicated by logic 1, to prevent power loss and heating.

In this phase of the study, we will address the pre-charge and pre-discharge stages. Consider a scenario in which a highly capacitive load is connected to the system initially. This load could be a high-power motor driver, inverter, or a similar system. Since the battery will be discharged, the pre-discharge process must be activated when the system starts up, allowing the capacitors of the load to fully charge. The current that is present at this particular point is referred to as the inrush current. It is imperative that this current be passed through a limiting resistor. This duration corresponds to approximately 5τ. This time depends on the capacitive and resistive values of the load.

Eq. (1) is the maximum precharge resistance is calculated to achieve the desired level of charge for the load capacitance within the specified timeframe. The actual precharge resistance employed may be less than this threshold, thereby expediting the precharging process but also augmenting power dissipation through the resistor.

$$R_{x_{max}} = \frac{T_{\max}}{nC} \tag{1}$$

The Rx is selected as the precharge resistor value. The maximum resistance calculated above can be utilized for this purpose. For instance, it can be employed to experiment with commercially available resistors or to expedite precharging processes.

Eq. (2) is the time constant for the RC circuit is determined by the following equation:

$$\tau = R_x C \tag{2}$$

This is the amount of time required to charge the capacitor to 63.2% of its maximum capacity. It is generally accepted that five-time constants are a reliable guideline for the optimal charging of a capacitor. In the event that the requisite standards are not met, the primary contactor may be susceptible to welding, which is a principal motivation underlying the present study. The solid-state switching method has been demonstrated to be effective in circumventing this issue. This can be adjusted by changing the precharging time input $T_{\max}$.

Eq. (3) is the precise temporal requirement for the precharging of the system to the desired level, employing the designated resistor value, must be ascertained. In the event that $R_{x_{max}}$ is utilized, the resultant time should equal the desired precharge time input.

$$T = nR_x C \tag{3}$$

Eq. (4) represents the number of time constants required to precharge the load capacitance to the desired percentage.

$$n = -ln|1 - q| \tag{4}$$

q is the percentage of the required system capacitance before the main switch closes.

With the Eq. (5) in this section, exponential charging equation will be applied to examine the capacitor voltage at time *t* that will increasing until reaching the source voltage. Subsequently, iteration calculations will be performed by writing the values of the system under study and comparing them with the simulation results.

$$V_C(t) = V_{batt}(1 - e^{-t/\tau}) \tag{5}$$

Voltage across the load capacitance at a time t after the commencement of precharging. This phenomenon is known as *"capacitance."*. *"e"* in this equation is referred to as Euler's equation and is approximately equal to 2.7183. *"t"* is refer to the time elapsed since the commencement of precharging is indicated.

Utilizing the above-listed equations and the values of the system incorporated in this study, the system parameters will be calculated. A comprehensive list of the system parameters can be found in Table 2 below.

Table 2. System Parameters

PARAMETERS	VALUE
Source Voltage	64V
Pre-Charge Resistor	47Ω
Load Capacitor	470 µF = 470 × 10^{-6} F
Initial Capacitor Voltage	0V
Time Constant	R·C = 22.09 ms

With the 470uF load capacitor and 47Ω limitation resistor, time constant τ is $470 \times 10^{-6} F \times 47\Omega = 0.02209$ second which is equal to 22.09 mili-second. The required number of time constant to charge the capacitor to 99.33% of its capacity can be determined using equation 4; $-ln|1 - 0.9933| = 5.00$. Therefore, it can be deduced that the capacitor is almost completely charged after five tau (τ) periods in the system under consideration. This period corresponds to 0.02209 milliseconds multiplied by five, which equals 110 milliseconds.

Table 3. Voltage at Key Time Points

Time (ms)	t/τ	$V_C(t) = V_{batt}(1 - e^{-t/\tau})$	Result (V)
t = 0	0	64·(1−1)	0
t = τ = 22.09 ms	1	64·(1−e^{-1})	40.41V
t = 2τ = 44.18 ms	2	64·(1−e^{-2})	55.91V
t = 3τ = 66.27 ms	3	64·(1−e^{-3})	61.12V
t = 4τ = 88.36 ms	4	64·(1−e^{-4})	63.63V
t = 5τ = 110.45 ms	5	64·(1−e^{-5})	63.79V ≅ 64V

The Eq. (6) will present the iteration that expresses the exponential decrease in the current passing through the resistance. Concurrently, the highest current value will be determined, and the results will be evaluated to ascertain whether the limits are being met. If the results indicate that improvements to the system are necessary, they will be implemented.

$$I(t) = \frac{V}{R} \times e^{-t/\tau} \quad (6)$$

Substitution of the battery voltage and pre-discharge resistance values into the aforementioned equation will allow for observation of the current change in the 0-5 τ time interval.

Table 4. Current Value Through Resistor

Time (ms)	t/τ	I(t) (A)
t = 0	0	1.362A
t = τ = 22.09 ms	1	0.501A
t = 2τ = 44.18 ms	2	0.184A
t = 3τ = 66.27 ms	3	0.068A
t = 4τ = 88.36 ms	4	0.025A
t = 5τ = 110.45 ms	5	0.009A

The capacitor's charge increases exponentially from 0 V to 64 V. The time constant, denoted by τ, determines the rate at which this process occurs. At 5τ, the capacitor reaches a state of over 99% charge accumulation, and the current undergoes exponential decay, commencing at 1.36 A and decreasing towards 0.

2.1.1. Simulation Results of Transient Power Paths

In order to simulate the pre-discharge event in the transient power path circuit (see Figure 2), it is necessary to connect a 470uF electrolytic capacitor, as illustrated in Figure 3. All values to be utilized at this stage have been previously defined in the preceding section, and the requisite calculations have been executed.

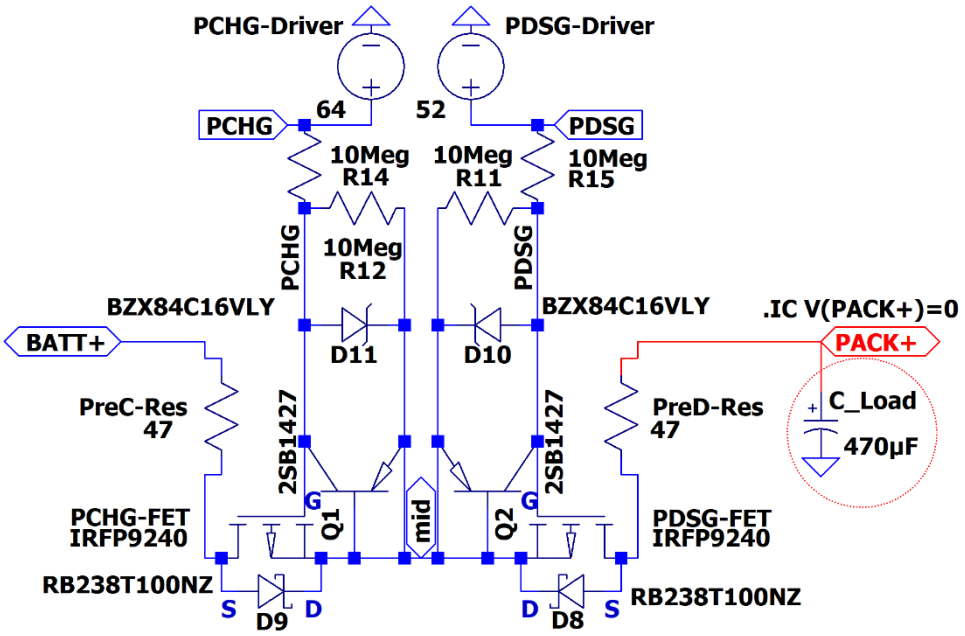

Figure 3. Load Connection of Pre-Discharge Path

As illustrated in Figure 3, a load capacitor connected in series with a 47Ω limiting resistor is depicted within a red circle. During the utilization of the transient power paths, the primary current attains the "mid" via a low impedance, thereby enabling bidirectional flow from that point, contingent upon the direction aligning with BATT+ or PACK+. However, it should be noted that this phenomenon occurs in a unidirectional manner, manifesting exclusively in response to a specific event. The device exhibits the capacity to execute pre-charging or pre-discharging operations; however, it does not possess the capability to perform both functions concurrently.

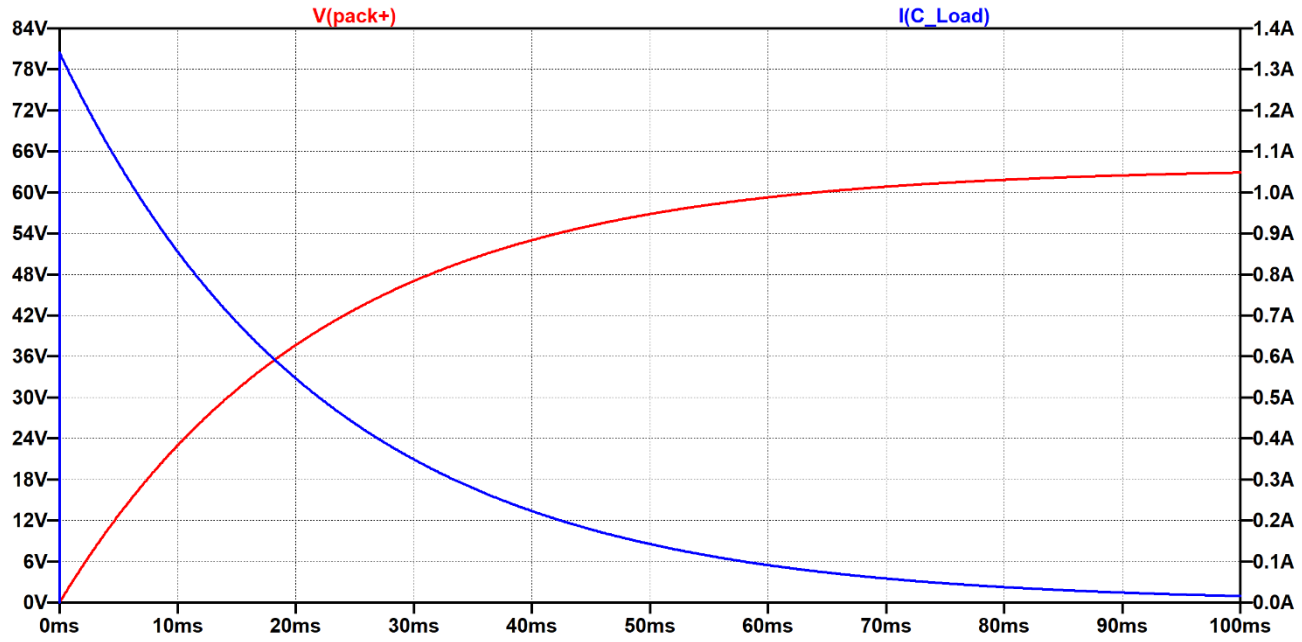

Figure 4. Simulation Results of Pre-Discharge

As illustrated in Figure 4, it is evident that the current demanded by the load consisting of a capacitor exhibits a decrease in accordance with the calculated iteration values, ultimately reaching 0 at the predetermined time. The blue graph labeled "I(C_load)" provides a visual representation of this phenomenon. In order to make this observation, it is necessary to take the right wall of the relevant graph into account. As can be seen, the right wall of the graph carries the current values, while the left wall carries the voltage values. The x-axis of the graph represents time. From an alternative perspective, the capacitor voltage attains the battery source voltage of 64V within the same interval of 110 milliseconds, as determined by the calculated iterations. The red graph, labeled V(pack+), is a representation of the voltage.

In the event of an inverse application of this circuit, it is imperative to operate a pre-charge circuit that is symmetrical to the pre-discharge circuit. The symmetry of the circuits is facilitated by the implementation of MOSFETs arranged in a back-to-back configuration. Consequently, there have been virtually no practical changes during the application stages. The initiation of this process is contingent upon the timing of the charging device's delivery of charging current to the battery, which should occur at a time that is distinct from the draw of load current from the battery. Alternatively, the process can be initiated immediately upon the establishment of a connection between the charging device and the battery. In the event that the charging device is equipped with its own switching capabilities, it is imperative that the pre-charge circuit be activated at the onset of the charging process. Consequently, this procedure is designated as pre-charging. In general, this sequence is not frequently employed in the context of automotive and industrial lithium battery applications. The objective of this study is to identify vulnerabilities in the system and implement supplementary safety measures to optimize the protection of life and property. While a battery, in its capacity as a load, does not exhibit the characteristics of a capacitor and does not necessitate inrush current, this observation does not guarantee the reliability of charging devices and voltage sources. There are substantial observational results indicating the preference of voltage sources over charging devices in battery charging applications, which is in direct contravention of established safety standards. In essence, the battery's internal resistance is minimal, which, in conjunction with the potential for a short circuit, could result in grave consequences. Notwithstanding the absence of a short circuit, this possibility must be assessed at the commencement of charging, and charging should only recommence once it has been confirmed that it is safe to do so. It is a highly safe choice to wait until it is determined that this situation does not apply and to continue the charging process via a low-impedance path.

2.2. Continuous Power Paths

Steady-state current paths are defined as the pathways through which currents that have left the transient region are transported. These currents are now constrained within the system's boundaries, have been deemed safe, and have stabilized at a particular value. These pathways are characterized by low impedance, resulting in minimal loss, and persist until the conclusion of the process.

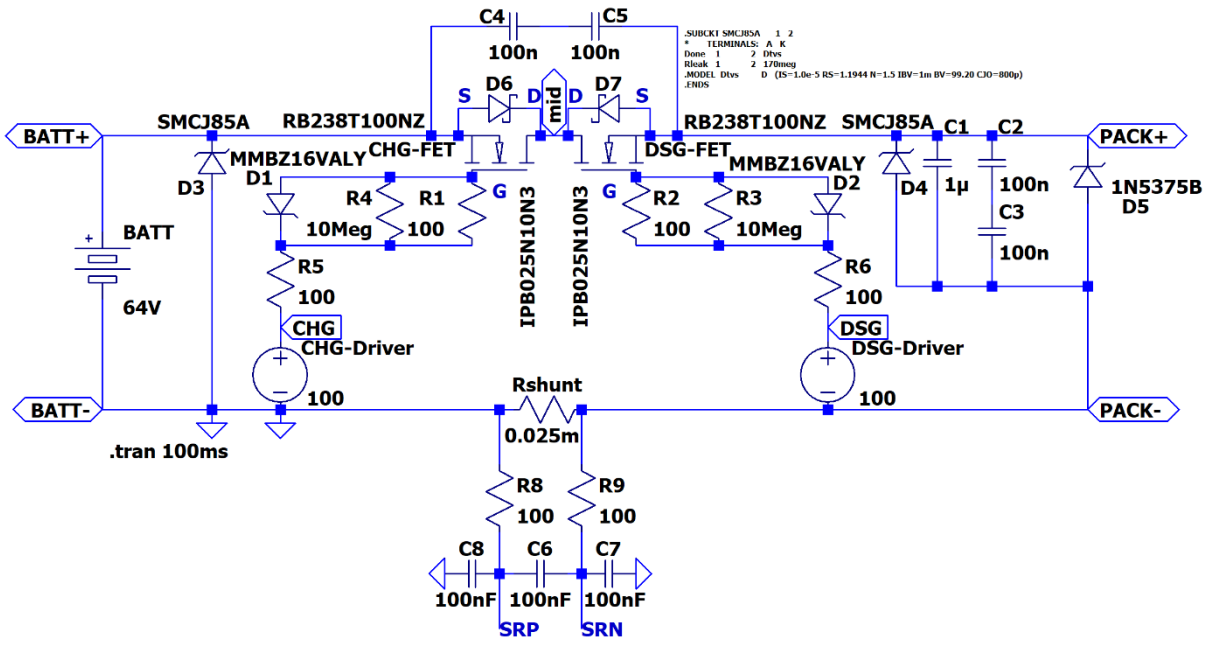

Figure 4. Steady-State Current Paths

Although the circuit in Figure 4 appears more complex than a conventional contactor design, it is a more effective and practical solution. It has a smaller footprint, is less expensive, is easier to control, has a longer service life, and can monitor current magnitude via the shunt resistor. The internal body diodes in the MOSFETs are placed back-to-back and face each other, acting as a barrier on that line. This creates excessive impedance on the line, which prevents current flow when the MOSFETs are not conducting. This feature isolates the battery and load on the line from each other.

Since our battery voltage is 64 volts and our goal is to achieve minimum impedance in the steady state, let's select an ohmic load with a value of 64 ohms to simplify the calculations.

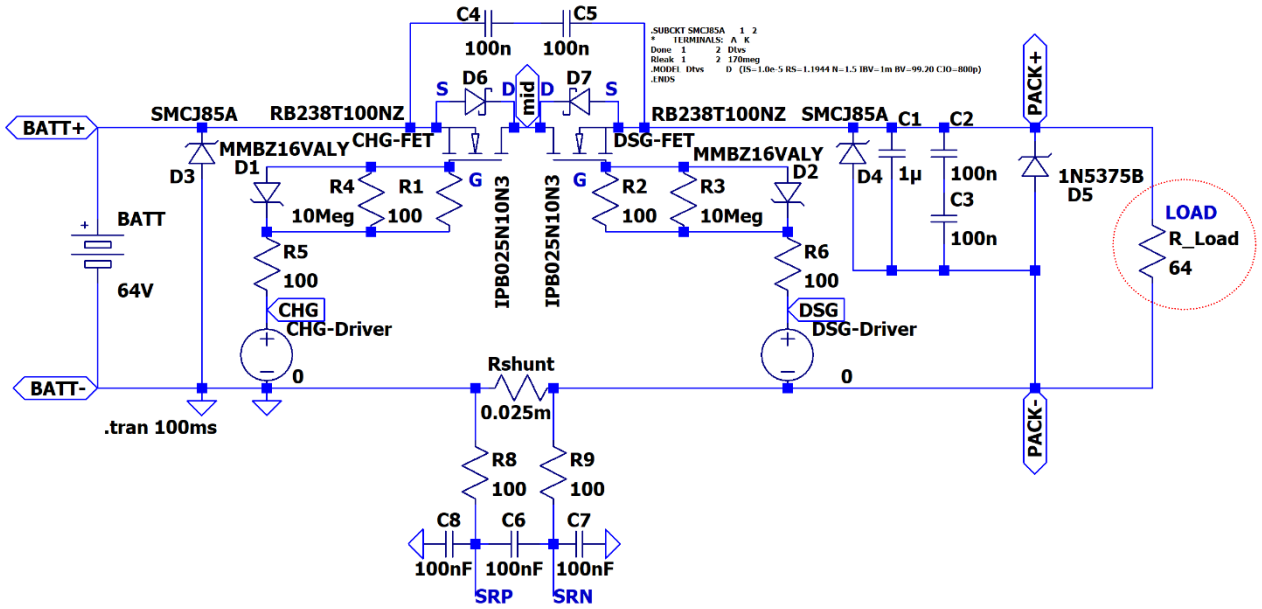

Figure 5. Load Connected Current Paths

As illustrated in Figure 5 above, a resistive load equal to the battery voltage is connected to the system. The objective is to utilize the fundamental equation for current, voltage, and resistance to ascertain the value of 1A that is expected to flow through the system.

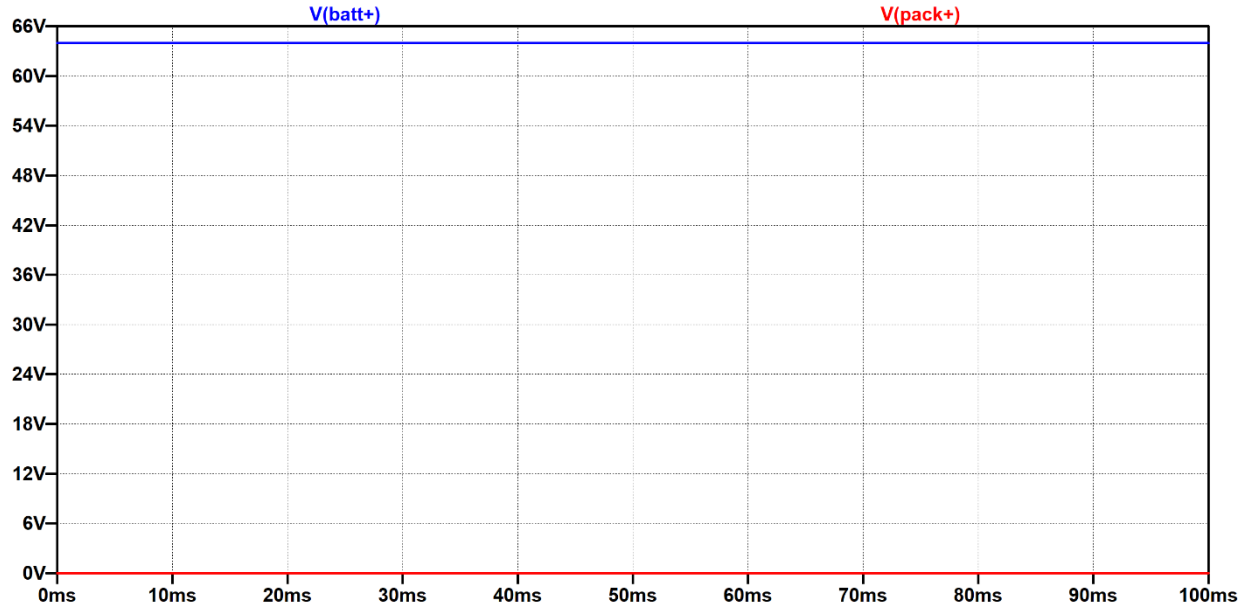

Figure 6. Battery Voltage and Load Voltage

As illustrated in Figure 6 above, despite the battery voltage measuring at 64V, the load voltage registers at 0 volts. This suggests that while the load is physically connected to the system, it is effectively isolated from the battery. In this position, the charge and discharge MOSFETs are deactivated. The subsequent step involves actuating the MOSFETs.

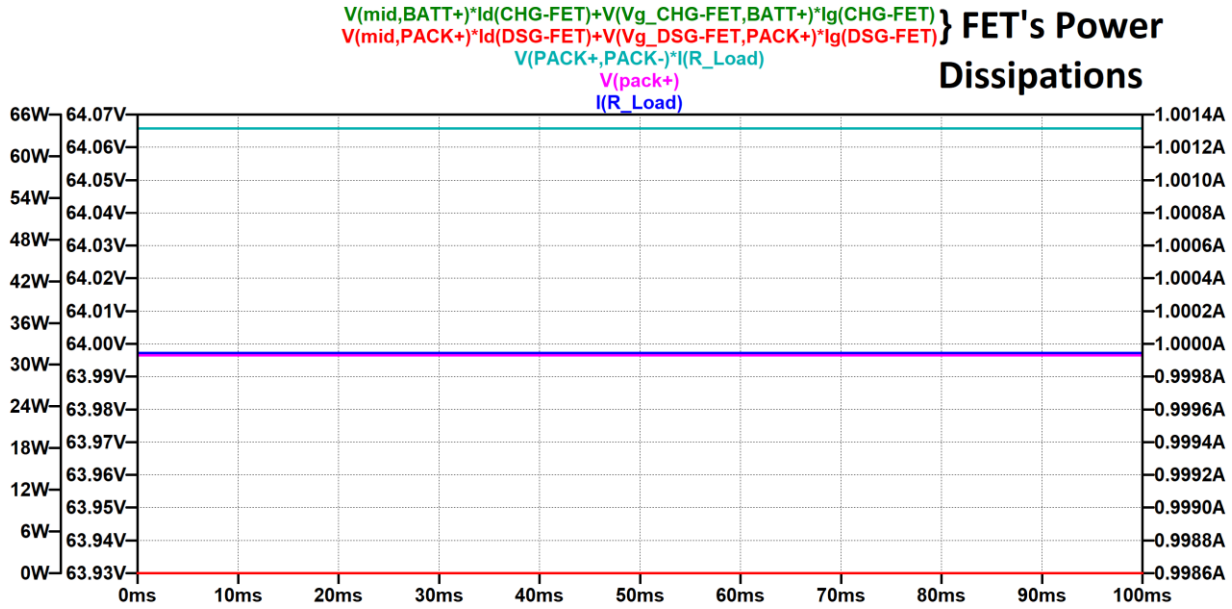

Figure 6. Load Current and Power Consumption

As illustrated in Figure 6, the current flowing through the load and the power consumed are depicted when both the charging and discharging MOSFETs are in the open position. In order to augment the system's current capacity, it is possible to increase the number of MOSFETs in parallel. However, it should be noted that in this particular simulation, only a single MOSFET is illustrated on each side. In real-world applications, the increase in the number of parallel MOSFETs in each branch results in enhanced power and current carrying capacities of the system. Concurrently, the internal resistances of the MOSFETs decrease in proportion when they are fully open, thereby reducing losses. The parallel connection limit is directly proportional to the switching capacity of the gate driver. Therefore, it is essential to ensure that the driver can reliably drive all MOSFETs. Furthermore, it is imperative to ensure that the number of MOSFETs in each branch is equal to prevent uneven internal resistance distribution, which has the potential to reduce the lifespan of the system.

3. Insulation Resistance Measurement

This apparatus is utilized for the uninterrupted surveillance of insulation resistance within electrical systems. The primary function of this technology is to ensure system safety by detecting the formation of leakage currents at an early stage, with a particular emphasis on areas where insulation levels are of paramount importance.

Isolation monitoring devices are utilized to assess the insulation resistance between the system and ground in electrical circuits. This evaluation aims to identify the presence of leakage currents. This is of particular importance for human safety and the protection of equipment. The device has been programmed to sound an alarm when the insulation level falls below a predefined threshold value. This approach enables the implementation of preventative measures prior to the exacerbation of the issue. In the event of insulation loss, the necessary precautions can be taken to prevent damage to the equipment in the system. This approach also mitigates the costly downtime that can result from equipment malfunctions. Electrical systems present a potential hazard to human life due to the occurrence of leakage currents. The implementation of insulation monitoring devices serves to mitigate the aforementioned risks, thereby promoting enhanced safety for both workers and users. Insulation defects can result in energy dissipation. The implementation of insulation monitoring devices serves to mitigate these losses, thereby enhancing the energy efficiency of the system.

It is imperative to engage in uninterrupted observation of the insulation level in battery systems for the purposes of ensuring safety and optimizing performance.

In this study, a circuit will be designed to measure leakage resistance in electric vehicles. In the initial phase, the battery voltage will be decreased to a level that is compatible with the microcontroller's readability capabilities. This reduction will be accomplished through the utilization of a voltage divider. A buffer op-amp will be utilized on the positive side of the main voltage line in the circuit.

This configuration is designed to facilitate enhanced signal clarity by ensuring minimal current draw from the signal source. This is accomplished through the op-amp's high input impedance and low output impedance, which together ensure that the signal source is not subject to significant current draw. The incorporation of an inverting operational amplifier within the circuit is imperative, as direct voltage measurement along the negative voltage line is not feasible. Furthermore, the implementation of protection and filter circuits is intended to enhance the reliability of the overall circuit configuration.

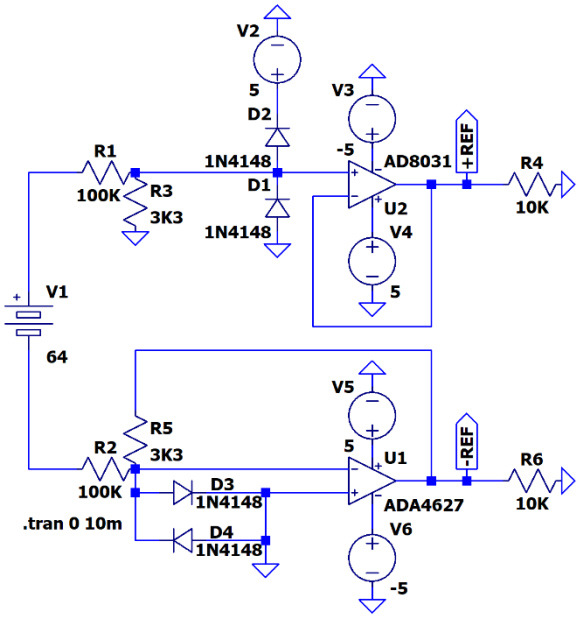

Figure 7. Insulation Leakage Monitoring Circuit

As illustrated in Figure 7, the configuration in question features an insulation resistance monitoring circuit devoid of leakage resistance. The reference terminals are categorized into two distinct groups: positive and negative. In the absence of leakage resistance, the voltages at these two terminals are required to be equal. The salient point is that the op-amp output value on the terminal with insulation loss decreases. This detail is of the utmost importance.

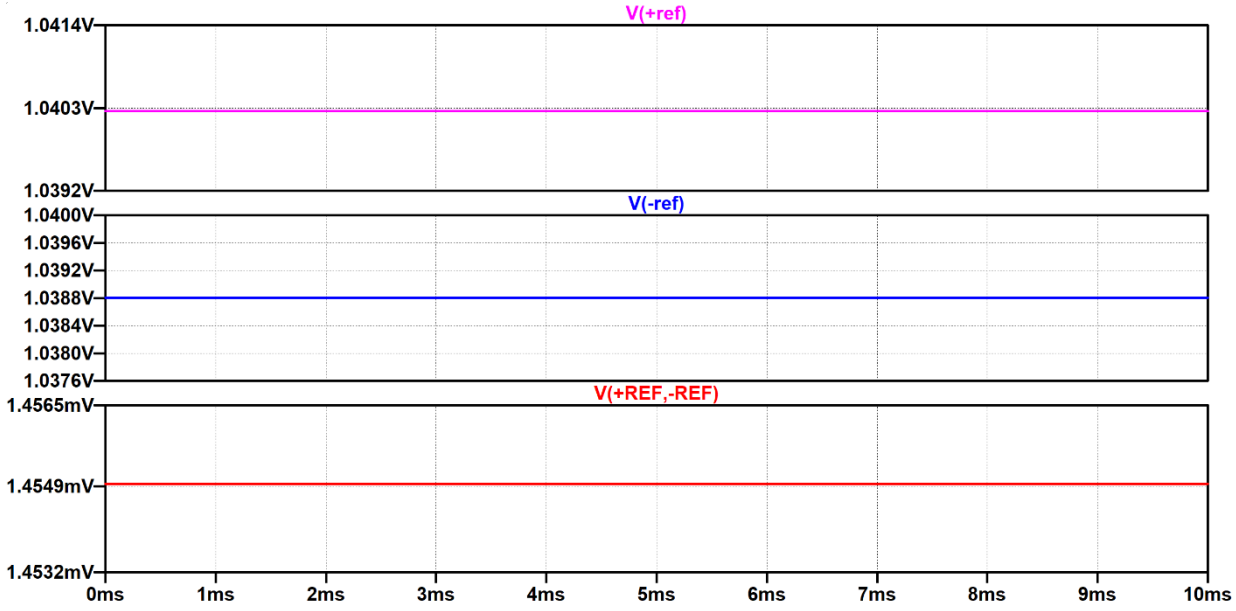

Figure 8. Reference Nets Voltage Measurements, No Leakage

As illustrated in Figure 8, the three graphs present the positive terminal reference voltage which is 1V, the negative terminal reference voltage which is 1V, and the potential difference between these two reference voltages, respectively. This voltage difference indicates that the insulation of the system is sufficiently safe and that both terminal ends have the same voltage value.

As previously stated, the applicable standard dictates that the insulation resistance must be 500 ohms per volt. Given the utilization of a 64V battery within the system, this value is determined to be 32 kohms. The subsequent step in this process will involve the implementation of 32Kohm leakage resistors at the positive and negative terminals, followed by a re-examination of the graphs.

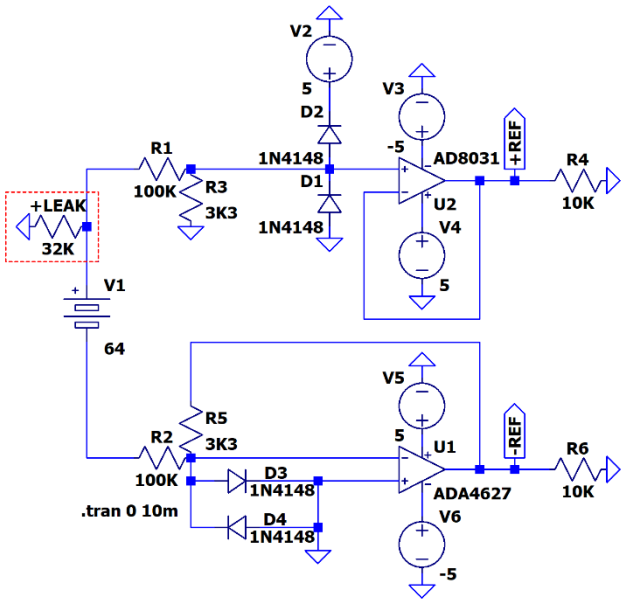

Figure 9. 32K +LEAK Resistor Applied

As illustrated in Figure 9, a leakage resistance of 32K has been implemented within the red dotted rectangle on the positive side. The graphs are presented in the same sequence in Figure 10 below.

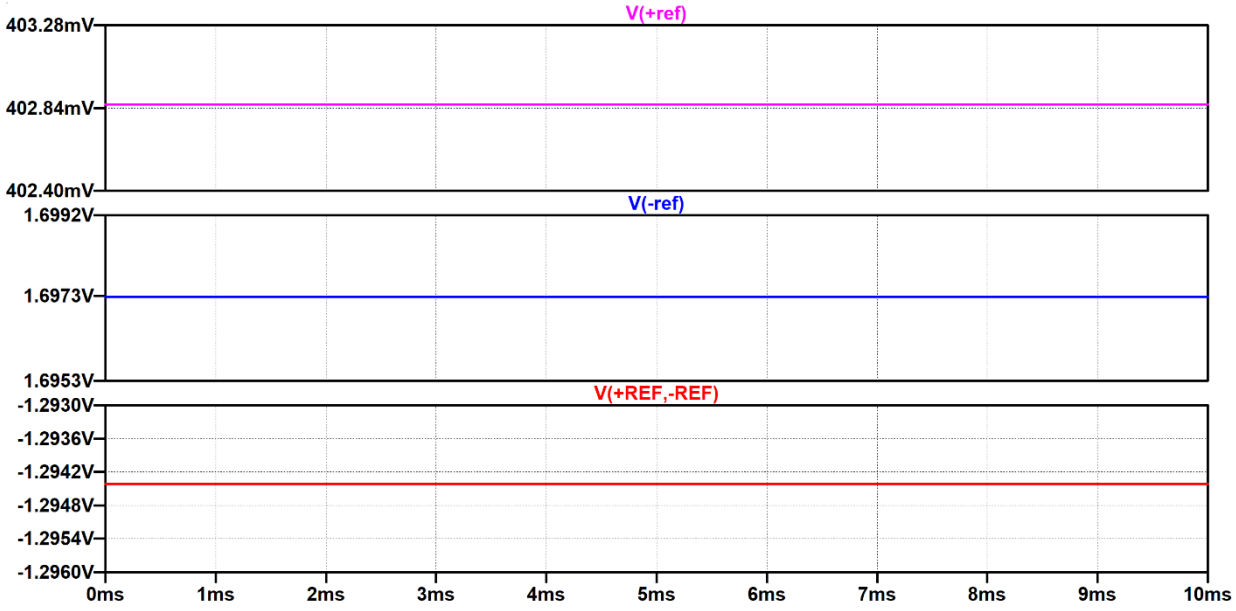

Figure 10. Reference Nets Voltage Measurements, Positive Leakage

As illustrated in image 10, the positive side of the opamp output experiences a decrease due to the leakage resistance being positioned on the positive side.

It is now necessary to repeat the aforementioned process for the negative side.

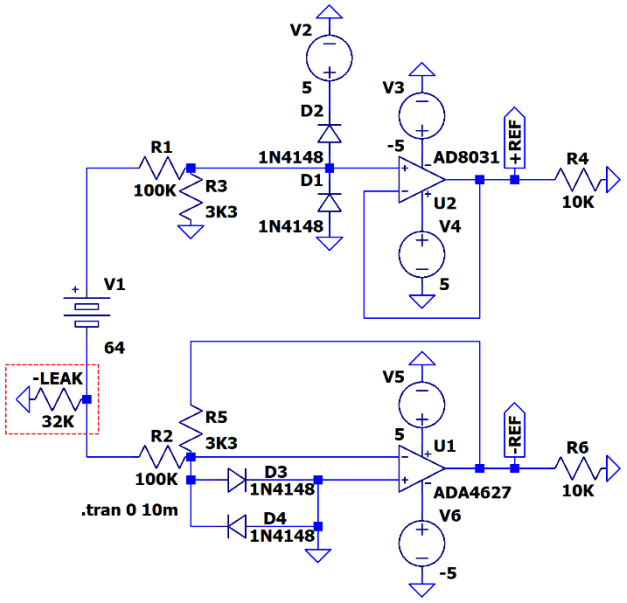

Figure 10. 32K -LEAK Resistor Applied

As illustrated in Figure 10, a leakage resistance of 32K has been implemented within the red dotted rectangle on the negative side. The graphs are presented in the same sequence in Figure 11 below.

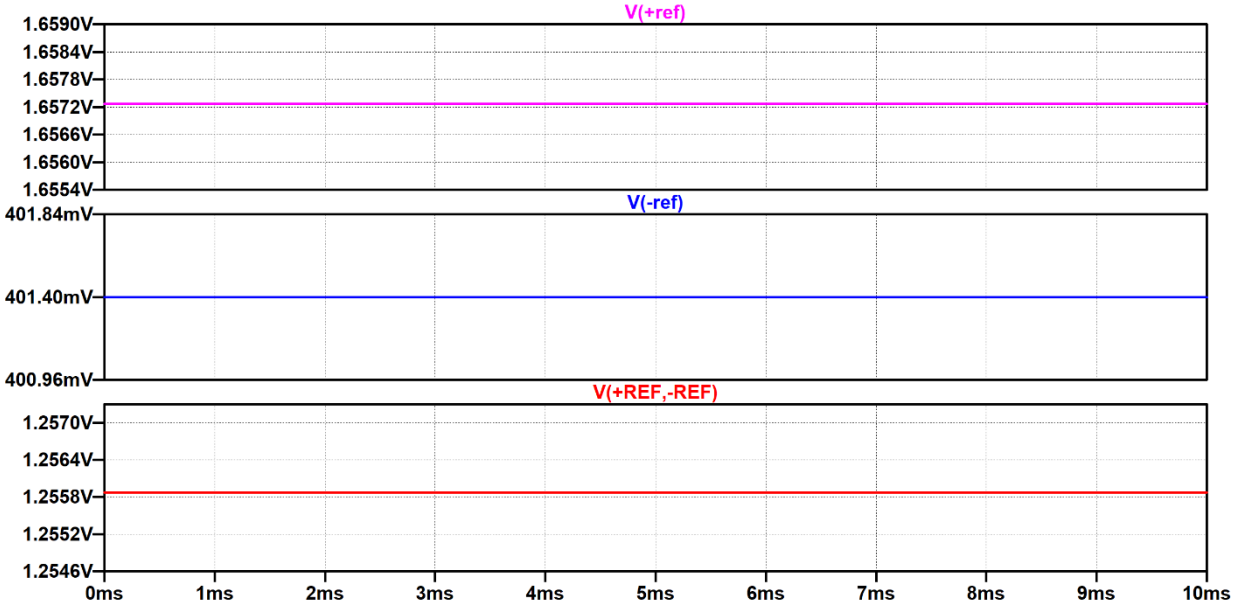

Figure 11. Reference Nets Voltage Measurements, Negative Leakage

As illustrated in Figure 11, it is evident that all results are reversed relative to the positive side, thereby validating the accuracy of the predictions.

4. Current Measurement with Kelvin-Connected Shunt Resistors and Electronic Fuses (eFuse)

The Kelvin connection is a four-terminal method employed to minimize measurement errors, particularly when measuring current through low-resistance shunts. Two terminals pass through the high-current path, while the remaining two terminals directly detect the potential difference at the measurement point. This ensures that potential drops in the conductive path and solder joints are not included in the measurement. Typically, integrated circuits such as a Battery Management System (BMS) or Analog Front-End (AFE) perform this measurement directly using SRN (Shunt Resistor Negative) and SRP (Shunt Resistor Positive) pins.

E-Fuse systems have been demonstrated to provide faster and more accurate protection in comparison to traditional fuses. For instance, in the event of a short circuit, these advanced devices can respond in less than 100 microseconds, whereas traditional fuses respond in milliseconds. This configuration is designed to prevent other systems in the power distribution line from shutting down or being damaged due to a short circuit. Furthermore, advanced technologies such as VIP-Fuse are employed to monitor the thermal limits of the wire in real time. The real-time effective current (IRMS) is measured by a shunt resistor, and the thermal limits of the wire are determined based on this measurement. When the current exceeds a certain threshold (INOM), the fuse is tripped by the system. This process is designed to prevent overheating in the wiring, thereby enhancing system safety.

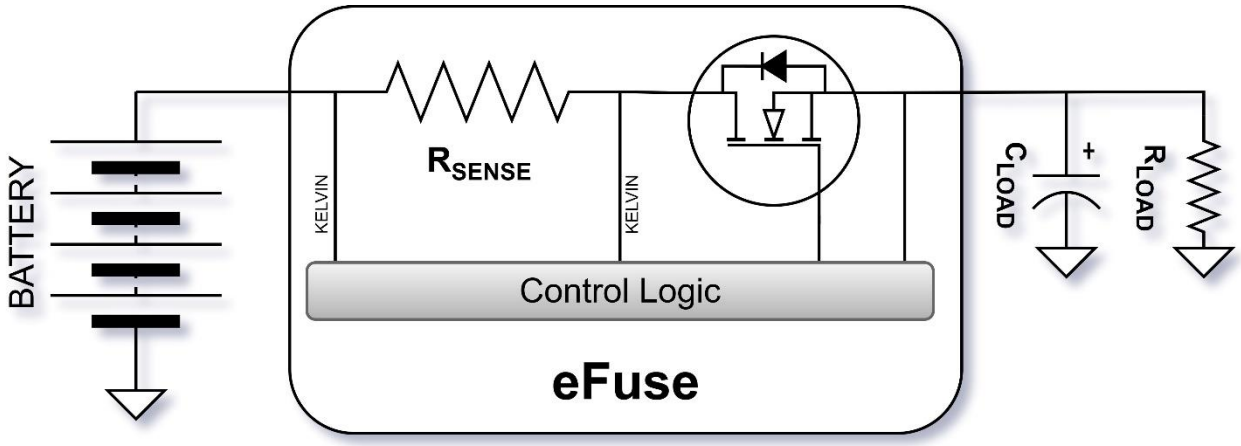

Figure 12. eFuse Schematic Design

A notable benefit of electronic fuses is their capacity to function through software-based algorithms. These algorithms calculate the wire's temperature based on measured current data using an electrode thermal model and trigger the fuse when a predetermined energy or heat limit is exceeded. However, in scenarios where there are discrepancies between these algorithms or when there is a dynamic current profile in the system, selectivity concerns may emerge between sequentially positioned e-Fuses. In such cases, while the objective is to trigger only the fuse closest to the fault, triggering the upstream fuses can result in a serious system outage.

To ensure the optimal functionality of these structures, meticulous attention must be accorded to the selection of shunt resistors and the configuration of e-Fuse algorithms. This is particularly salient in the context of automotive applications that prioritize stringent safety targets, such as ASIL-D. In such scenarios, the implementation of robust hardware and software protection systems is of paramount importance.

5. Conclusions

The present study proposes a multi-purpose electronic contactor system, integrating a high-side N-channel FET driver architecture, precision shunt-based bilateral current sensing, and robust insulation resistance monitoring in accordance with EV safety standards. The proposed solution involves the replacement of traditional electromechanical contactors with a solid-state alternative. This modification has been shown to enhance system responsiveness, safety, and integration potential for modern E/E architectures. The pre-charge and pre-discharge circuits are modeled and verified analytically and experimentally, ensuring inrush current limitations within safe thermal margins. Real-time current measurement is achieved using Kelvin-connected low-resistance shunt resistors and a differential AFE interface, providing accurate data for system control and protection.

Additionally, the insulation resistance monitoring system employs a dynamic bridge method and is in accordance with the UNECE R100 regulation's 500 Ω/V threshold. The design incorporates a dual measurement approach and compensates for distributed capacitance and environmental variables. This ensures accurate online detection of insulation degradation, even under adverse operational conditions.

Complementary electronic fuse (eFuse) modules, based on programmable thresholds and high-speed overcurrent detection (<100 μs), provide adaptive and resettable protection against transient faults. This, in turn, supports selective protection and wire harness safety per the latest zonal E/E architecture paradigms.

Through the utilization of analytical modeling, LTspice simulations, and real-world validation, the integrated system exhibits reduced switching losses, enhanced measurement resolution, and augmented fail-operational behavior, making it suitable for next-generation EV platforms. This work contributes a compact, scalable, and regulation-aligned solution poised for integration into EV BDU and power control systems, directly supporting the digitalization and safety goals of automotive electrification.

Nomenclature

AFE	Electrical Vehicle
BMS	Battery Management System
CHG	Charge
DC	Direct Current
DSG	Discharge
E/E	Electrical and Electronics
eFuse	Electronic Fuse
EV	Electrical Vehicle
FET	Field-Effect Transistor
IRMS	Root Mean Square Current
MOS	Metal-Oxide-Semiconductor
PCHG	Pre-Charge
PDSG	Pre-Discharge
SRN	Shunt Resistor Negative
SRP	Shunt Resistor Positive
V	Voltage (V)
I	Current (A)
R	Resistance (Ω)
C	Capacitance (F)
τ	Time Constant (s)
q	Percentage od capacitor charge (%)
t	Time (s)

References

[1] M. Sivaramkrishnan, N. P, S. K, G. S and S. N, "Smart Electric Vehicle with Safety System," *2023 International Conference on Self Sustainable Artificial Intelligence Systems (ICSSAS)*, Erode, India, 2023, pp. 1488-1493, doi: 10.1109/ICSSAS57918.2023.10331868.

[2] A. Masakure, A. Gill and M. Singh, "The Impact of Battery Charging and Discharging Current Limits on EV Battery Degradation and Safety," *2023 3rd Asian Conference on Innovation in Technology (ASIANCON)*, Ravet IN, India, 2023, pp. 1-5, doi: 10.1109/ASIANCON58793.2023.10270635.

[3] Guo, Feng, Danping She, Xinfeng Zhang, and Yue Han. 2025. "Design of a High-Voltage Insulation Resistance Detection System for Commercial Vehicles" *Batteries* 11, no. 4: 143. https://doi.org/10.3390/batteries11040143

[4] "IEEE Master Test Guide for Electrical Measurements in Power Circuits," in *IEEE Std 120-2023 (Revision of IEEE Std 120-1989)* , vol., no., pp.1-118, 10 June 2024, doi: 10.1109/IEEESTD.2024.10552208.

[5] Y. Zou, X. Chen, P. He, Z. Guo, H. Mo and Y. Su, "Research on Multi-function Insulation Resistance Tester," *2023 3rd International Conference on Energy Engineering and Power Systems (EEPS)*, Dali, China, 2023, pp. 811-815, doi: 10.1109/EEPS58791.2023.10256806.

[6] Taha Al-Dulaimi, "Insulation Resistance Measurement in Automotive Environment", *Metropolia University of Applied Sciences*, Bachelor of Engineering, Automotive Engineering, Bachelor's Thesis, 13 March 2025

[7] Qiqi Dai, Zhongwen Zhu, Denggao Huang, Mingxing Du, Kexin Wei; Insulation detection of electric vehicle batteries. *AIP Conf. Proc.* 7 June 2018; 1971 (1): 040021. https://doi.org/10.1063/1.5041163

[8] Y.-H. Chiang and W.-Y. Sean, 'Adaptive Control for Estimating Insulation Resistance of High- Voltage Battery System in Electric Vehicles', *New Trends in Electrical Vehicle Powertrains.* IntechOpen, Jan. 30, 2019. doi: 10.5772/intechopen.75468.

[9] E. Dincer and A. B. Yildiz, "Design of FET Based Electronic Power Path Controller for Lithium Battery Applications," *2024 IEEE 3rd International Conference on Electrical Power and Energy Systems (ICEPES)*, Bhopal, India, 2024, pp. 1-6, doi: 10.1109/ICEPES60647.2024.10653532.

[10] M. A. Hannan, M. M. Hoque, A. Hussain, Y. Yusof and P. J. Ker, "State-of-the-Art and Energy Management System of Lithium-Ion Batteries in Electric Vehicle Applications: Issues and Recommendations," in *IEEE Access*, vol. 6, pp. 19362-19378, 2018, doi: 10.1109/ACCESS.2018.2817655.

[11] A. Soldati, E. Imamovic and C. Concari, "Bidirectional Bootstrapped Gate Driver for High-Density SiC-Based Automotive DC/DC Converters," in *IEEE Journal of Emerging and Selected Topics in Power Electronics*, vol. 8, no. 1, pp. 475-485, March 2020, doi: 10.1109/JESTPE.2019.2955004.

[12] T. Langbauer, A. Connaughton, F. Vollmaier and K. Krischan, "Pre-Charging of a DC-Link Capacitor from a High Voltage Battery," *2020 IEEE 21st Workshop on Control and Modeling for Power Electronics (COMPEL)*, Aalborg, Denmark, 2020, pp. 1-6, doi: 10.1109/COMPEL49091.2020.9265799.

[13] Magar, P., Deshpande, R., Shinde, R., Deo, M. et al., "Analysis of Semiconductor Based Pre-charge & Cut-off Circuits for 2W/3W Electric Vehicle Battery Management Systems," *SAE Technical Paper* 2021-26-0168, 2021, https://doi.org/10.4271/2021-26-0168.

[14] Surachai Wongfookeat, Thanatchai Kulworawanichpong, "Outrush Current Control by Hot Swap Controller for Battery Protection in Electrical Vehicle", Energy Procedia, Volume 138, 2017, Pages 87-92, ISSN 1876-6102, https://doi.org/10.1016/j.egypro.2017.10.063.

[15] Eun-Ju Lee, Jung-Hoon Ahn, Seung-Min Shin and Byoung-Kuk Lee, "Comparative analysis of active inrush current limiter for high-voltage DC power supply system," *2012 IEEE Vehicle Power and Propulsion Conference*, Seoul, 2012, pp. 1256-1260, doi: 10.1109/VPPC.2012.6422710.

[16] Ozguc, M., Ipek, E., Aras, K., & Erhan, K. (2019). Comprehensive Analysis of Pre-Charge Sequence in Automotive Battery Systems. *Transactions on Environment and Electrical Engineering*, *4*(1), 1-6. doi:http://dx.doi.org/10.22149/teee.v4i1.136

[17] R. Letor and R. Crisafulli, "Smart Power devices and new electronic fuses compliant with new E/E architecture for autonomous driving," *2019 AEIT International Conference of Electrical and Electronic Technologies for Automotive (AEIT AUTOMOTIVE)*, Turin, Italy, 2019, pp. 1-6, doi: 10.23919/EETA.2019.8804538.

[18] C. Mayer, M. Baumann and H. -G. Herzog, "Analytic Selectivity Evaluation of Vehicular Electronic Fuses' Wire Protection Algorithms," *2024 IEEE Transportation Electrification Conference and Expo (ITEC)*, Chicago, IL, USA, 2024, pp. 1-6, doi: 10.1109/ITEC60657.2024.10598941.